MRI of Chronic Obstructive Pulmonary Disease

Julia Ley-Zaporozhan and Edwin JR van Beek

Contents

J. Ley-Zaporozhan, M.D. (✉)
Institute for Clinical Radiology,
Ludwig-Maximilians University of Munich,
Lindwurmstrasse 4, 80337 Munich, Germany
e-mail: julia.leyzaporozhan@gmail.com

E.J. van Beek, M.D., Ph.D.
Edinburgh Imaging, Queen's Medical Research
Institute, University of Edinburgh,
47 Little France Crescent, Edinburgh EH16 4TJ, UK
e-mail: edwin-vanbeek@ed.ac.uk

Key Points

MRI is becoming increasingly useful for imaging of lung structure and function, in terms of airway imaging, assessment of ventilation, and evaluation of lung perfusion and right heart function. This modality is highly versatile and capable of generating a range of inherent and exogenously introduced contrast mechanisms while maintaining high resolution as well as incredible speed of data acquisition.

It is quite likely that MRI techniques will allow further evaluation of physiological and pathophysiological aspects of COPD, and this should ultimately lead to improved understanding and treatment of this complex heterogeneous disease.

1   Introduction

Chronic obstructive pulmonary disease (COPD) is the fourth most common cause of death among adults (Rabe et al. 2007). COPD is characterized by incompletely reversible (usually progressive) airflow limitation, which is associated with an abnormal inflammatory response of the lung to noxious particles or gases. It is caused by a mixture of airway obstruction (obstructive bronchiolitis) and parenchymal destruction (emphysema), the relative contributions of which are variable (Rabe et al. 2007). Chronic bronchitis, or the presence of cough and sputum production for at

least 3 months in each of the 2 consecutive years, remains a clinically and epidemiologically useful diagnostic classifying term. Pulmonary emphysema is a pathological term and is defined by the American Thoracic Society as an abnormal permanent enlargement of the air spaces distal to the terminal bronchioles, accompanied by the destruction of their walls. In a simplified way, obstructive airflow limitation leads to air trapping with subsequent hyperinflation of the airspaces, which combined with inflammatory lung injury leads to destruction of the lung parenchyma. For severity assessment of COPD lung function tests, such as forced expiration volume in 1 s (FEV_1), FEV_1/FVC (forced vital capacity) and diffusing capacity for carbon monoxide (DLco) are used. However, pulmonary function tests only provide a global measure without any regional information and are not suitable for determination of structural abnormalities or for distinguishing the causes of air outflow obstruction. Although extremely useful in clinical practice and for global management of patients, pulmonary function tests are known to be relatively insensitive to both early stages and small changes of manifest disease. Furthermore, pulmonary function tests are dependent upon the effort and compliance of the patient, and are difficult to be reliably performed in young children. Chronic hyperinflation impacts on diaphragmatic geometry with subsequent dysfunction due to dissociation of the breathing mechanics. The disease also affects the pulmonary arteries: intimal thickening, smooth muscle hypertrophy, and inflammation are described, which ultimately give rise to vascular remodeling (Szilasi et al. 2006). The direct vascular changes and hyperinflation lead to the precapillary type of pulmonary hypertension and pulmonary vascular flow disturbance (Rosenkranz 2007).

In contrast to pulmonary function tests, radiological imaging techniques may be able to differentiate the components of obstructive lung disease on a regional basis, with the possibility of detecting early disease stages prior to the onset of symptoms. Computed tomography (CT) is the mainstay diagnostic modality in this field with emphasis on structural imaging of lung parenchyma and airways. Magnetic resonance imaging (MRI) has the potential to provide regional information about the lung without the use of ionizing radiation, but is hampered by several challenges: the low amount of tissue relates to a small number of protons leading to low signal, countless air–tissue interfaces cause substantial susceptibility artifacts, and last but not least, respiratory and cardiac motion. In several lung diseases, such as tumors, the amount of protons or the blood volume is actually increased and motion is reduced, which provides better pre-conditions for MRI. In obstructive pulmonary disease, however, there are no facilitating disease-related effects as there is loss of tissue and reduced blood volume due to hypoxic vasoconstriction and the degree of hyperinflation has a negative correlation with the MR signal. The depiction of the airways by MRI is certainly limited to the central bronchi. Fortunately, MRI has shown significant potential beyond the mere visualization of structure by providing comprehensive information about "function," such as perfusion, hemodynamics, ventilation, and respiratory mechanics.

2 Parenchyma

The most frequently utilized sequences in MRI of COPD are acquired in a single breath-hold. The T2-weighted single-shot techniques with partial Fourier acquisition (HASTE) sequence in coronal and/or axial orientation allow for the depiction of pulmonary infiltrates, inflammatory bronchial wall thickening, and mucus collections (Figs. 1 and 2). T1-weighted 3D gradient echo sequences, such as volume-interpolated breath-hold examination (VIBE), are suitable for the assessment of the mediastinum and common nodular lesions. The intravenous application of contrast material markedly improves the diagnostic yield of T1-weighted sequences by a clearer depiction of vessels, hilar structures, and solid pathologies. A major goal in inflammatory obstructive airway disease is to differentiate inflammation within the wall from muscular hypertrophy, edema, and mucus collection which cannot be achieved by CT, but can be addressed

Fig. 1 Coronal CT reformats (**a**) and corresponding coronal T2-weighted (HASTE) images (**b**): severe emphysema with predominance of the right lower lobe on CT corresponds to a loss of MR signal (*arrows*) reflecting destruction of the parenchyma and rarefication of the pulmonary vasculature

by the use of T1- and T2-weighted images as well as contrast enhancement (Ley-Zaporozhan et al. 2008). Different MRI sequences were compared to CT for detection of the severity of emphysema and leading emphysema type on a lobar level. MRI matched the CT in only half of the cases: the sensitivity for emphysema severity was 44%, 48%, and 41%, and the leading type of emphysema was 68%, 55%, and 60% for T2w-HASTE, T1w-VIBE, and T1w-ce-VIBE, respectively (Ley-Zaporozhan et al. 2010). All sequences showed a similar diagnostic performance; however a combination of T2w-HASTE and ce-VIBE was recommended. The method proved very reproducible in a group of 19 patients, who were imaged on 2 consecutive days, resulting in a weighted kappa of 0.86, 95%CI = 0.81–0.91 (Jobst et al. 2015a).

The extent of hyperinflation and hypoxic vasoconstriction is directly associated with the loss of signal (Bankier et al. 2004). While emphysematous destruction can hardly be diagnosed by a loss of signal, it is much easier to detect hyperinflation just by the size or volume of the thorax.

Fig. 2 Coronal T2-weighted (HASTE) image shows the typical flattening of the diaphragm in emphysema

In one of the first studies, it was shown that the change of parenchymal signal intensity measured by multiple inversion-recovery sequence with a HASTE acquisition at inspiration and expiration correlates with FEV_1 ($r = 0.508$) and might warrant further studies as a predictor of airflow obstruction (Iwasawa et al. 2007).

Recently T1w VIBE was used in a few patients at different lung volumes (Pennati et al. 2014). After semiautomatic segmentation of lung parenchyma from the surrounding soft tissue, a deformable image registration algorithm was applied to follow the signal change between different inflation volumes, resulting in a map of ^1H signal change. These maps can be used for regional investigation of lung function.

In the last couple of years measurement of the lung density using ultrashort TE sequences showed promising results. These sequences significantly improve the pulmonary MR signal so that areas with less parenchyma can be visualized and quantified (Hoffman et al. 2016). In 15 patients with COPD the mean signal intensity of one coronal central slice showed good correlation with the amount of density-based emphysema from CT ($r = -0.71$) (Ma et al. 2015). Another

study on ten patients applied a 3D approach and defined emphysema at a threshold of <10% of mean thoracic soft-tissue signal to segment the lower signal regions from healthy lung. Emphysema amount measured on MRI and CT showed a high correlation ($r^2 = 0.79$) (Roach et al. 2016). In a larger study population of 40 smokers without COPD, UTE correlated with different clinical stages of COPD (Ohno et al. 2011). UTE-MRI with a short interval measured in 60 smokers without and with different clinical stages of COPD showed moderate correlation with CT ($r = 0.65$) and FEV1/FVC% ($r = 0.62$), and good correlation with FEV1% (0.75) and DLCO% ($r = 0.79$) (Ohno et al. 2014).

More recently T1 mapping using snapshot fast low angle shot (FLASH) was investigated as a potential biomarker in COPD. T1 was significantly shorter in 24 patients with COPD compared to 12 age-matched healthy volunteers (Alamidi et al. 2016). In a group of 20 patients with COPD, a strong correlation ($r = 0.81$) was found between T1 abnormalities and MR perfusion abnormalities using a zone-based approach (Fig. 3) (Jobst et al. 2015b).

3   Airways

Several pathological studies have shown that a major site of airway obstruction in patients with COPD is in airways smaller than 2 mm internal diameter (Hogg et al. 2004). The 2 mm airways are located between the 4th and the 14th generation of the tracheobronchial tree. Airflow limitation is closely associated with the severity of luminal occlusion by inflammatory exudates and thickening of the airway walls due to remodeling. Severe peripheral airflow obstruction can also affect the proximal airways from subsegmental bronchi to the trachea.

For assessment of tracheal instability MR cine acquisitions during continuous respiration or forced expiration are recommended (Heussel et al. 2004). The depiction of airway dimensions and thickness of the airway walls by MRI under physiological conditions is limited to the central bronchi. For depiction of the bronchiectasis high
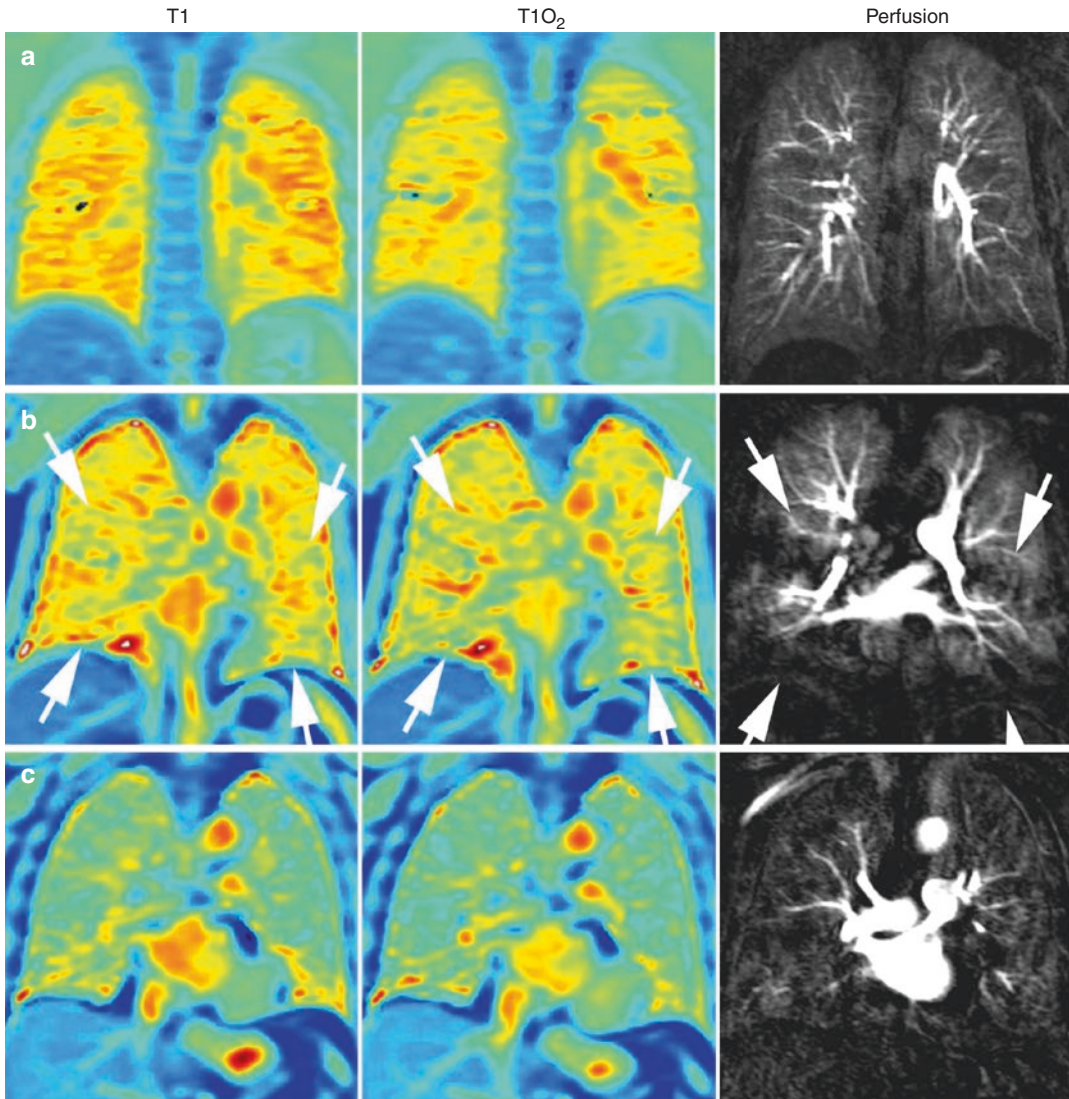
Fig. 3 Comparison of T1 and perfusion characteristics: Normal T1 mapping at room air (*left*), T1 mapping after 100% O2 (*middle*), and DCE lung perfusion (*right*) (zonal scores = 0 each) of a 29-year-old healthy volunteer (**a**). Fifty-nine-year-old patient with GOLD stage II showing minor T1 abnormalities at room air (score = 1), normal ΔT1 after 100% O2 (score = 0), and minor perfusion abnormalities (score = 1) of the middle and lower lung zones (area between *white arrows*), reflecting lung areas with intact ventilation and simultaneous perfusion impairment (**b**). Severe T1 abnormalities at room air, abnormal ΔT1 after 100% O2, and perfusion abnormalities (score = 2 each) affecting the entire lung of a 75-year-old patient with GOLD stage II (**c**). Reprinted with permission from Jobst et al. (2015a, b)

spatial resolution is essential. By using a 3D VIBE with a voxel size of approximately $0.9 \times 0.88 \times 2.5 \text{ mm}^3$ a sensitivity of 79% and a specificity of 98% regarding the visual depiction of bronchiectasis were shown compared to CT (Biederer et al. 2003).

4 Respiratory Dynamics

Respiration is the result of the complex interaction between chest wall and diaphragm motion, and it can be visualized by 2D or 3D dynamic MR techniques (Cluzel et al. 2000; Plathow

et al. 2004, 2005). For data acquisition time-resolved techniques are used, which can be based on FLASH or trueFISP sequences. This allows for a high temporal resolution down to 100 ms per frame.

Hyperinflation of the lung severely affects diaphragmatic geometry with subsequent reduction of the mechanical properties, while the effects on the mechanical advantage of the neck and rib cage muscles are less pronounced (Decramer 1997). The common clinical measurements of COPD do not provide insights into how structural alterations in the lung lead to dysfunction in the breathing mechanics, although treatments such as lung volume reduction surgery (LVRS) are thought to improve lung function by facilitating breathing mechanics and increasing elastic recoil (Henderson et al. 2007).

In contrast to normal subjects with regular, synchronous diaphragm and chest wall motion, dynamic MRI in patients with emphysema frequently showed reduced, irregular, or asynchronous motion, with a significant decrease in the maximum amplitude and the length of apposition of the diaphragm (Suga et al. 1999). In some patients the ventral portion of the hemidiaphragm moved downward at MRI while the dorsal part moved upward like a seesaw (Iwasawa et al. 2000). The paradoxical diaphragmatic motion correlated with hyperinflation, although severe hyperinflation tended to restrict both normal and paradoxical diaphragmatic motion (Iwasawa et al. 2002). Another study showed that the distribution of emphysema might have an influence on the diaphragmatic motion. The lower zone emphysema on CT correlated significantly with diaphragmatic flattening and abnormal chest wall motion evaluated with dynamic MRI whereas emphysema of the upper lung zone did not correlate with these parameters (Iwasawa et al. 2011). After LVRS, patients showed improvements in diaphragm and chest wall configuration and mobility at MRI (Suga et al. 1999). Ultrafast dynamic proton MRI was shown to be able to demonstrate the rapid volume changes observed during forced vital capacity maneuver (Fig. 4) and correlated closely with pulmonary function tests, but with the added

advantage of providing regional information on changes in lung volumes during this procedure (Swift et al. 2007; Eichinger et al. 2007).

5 Ventilation

As sufficient gas exchange depends on matched perfusion and ventilation, assessment of regional ventilation is important for the diagnosis and evaluation of pulmonary emphysema. The most established method for imaging regional lung ventilation is nuclear medicine studies using krypton-81m (Kr-81m), xenon-133 (Xe-133), radiolabeled aerosol (Technegas), and technetium-99m (Tc-99m)-labeled diethylentriamine-pentaacetic acid (DTPA). The utility of nuclear medicine in pulmonary diseases has been well documented. However, these techniques are hampered by low spatial and temporal resolution, and the necessity of inhalation of radioactive tracers. While 3D (SPECT) imaging requires approximately 20 min of imaging time, the diagnostic power of the technique is limited.

Although PFTs and nuclear medicine imaging have been established as the most common and reliable pulmonary function techniques, other techniques such as contrast-enhanced proton and hyperpolarized noble gas MRI are strong contenders in the functional imaging race. They provide a rapid, high-resolution regional quantification of disease progress and onset without the need for ionizing radiation tracers.

MRI signal changes inherent to lung tissue expansion and contraction that occur during normal breathing could be exploited to generate ventilation and perfusion maps. Fourier decomposition of the 1H signal intensity caused by compression and expansion of the lung parenchyma and pulmonary blood flow can be used to evaluate pulmonary ventilation and perfusion (Bauman et al. 2013). This method does not depend on inhaled gas or injected contrast agents. Despite these important advantages, there have been no large clinical COPD studies that have taken advantage of these novel pulmonary 1H MRI measurements (Coxson et al. 2014).
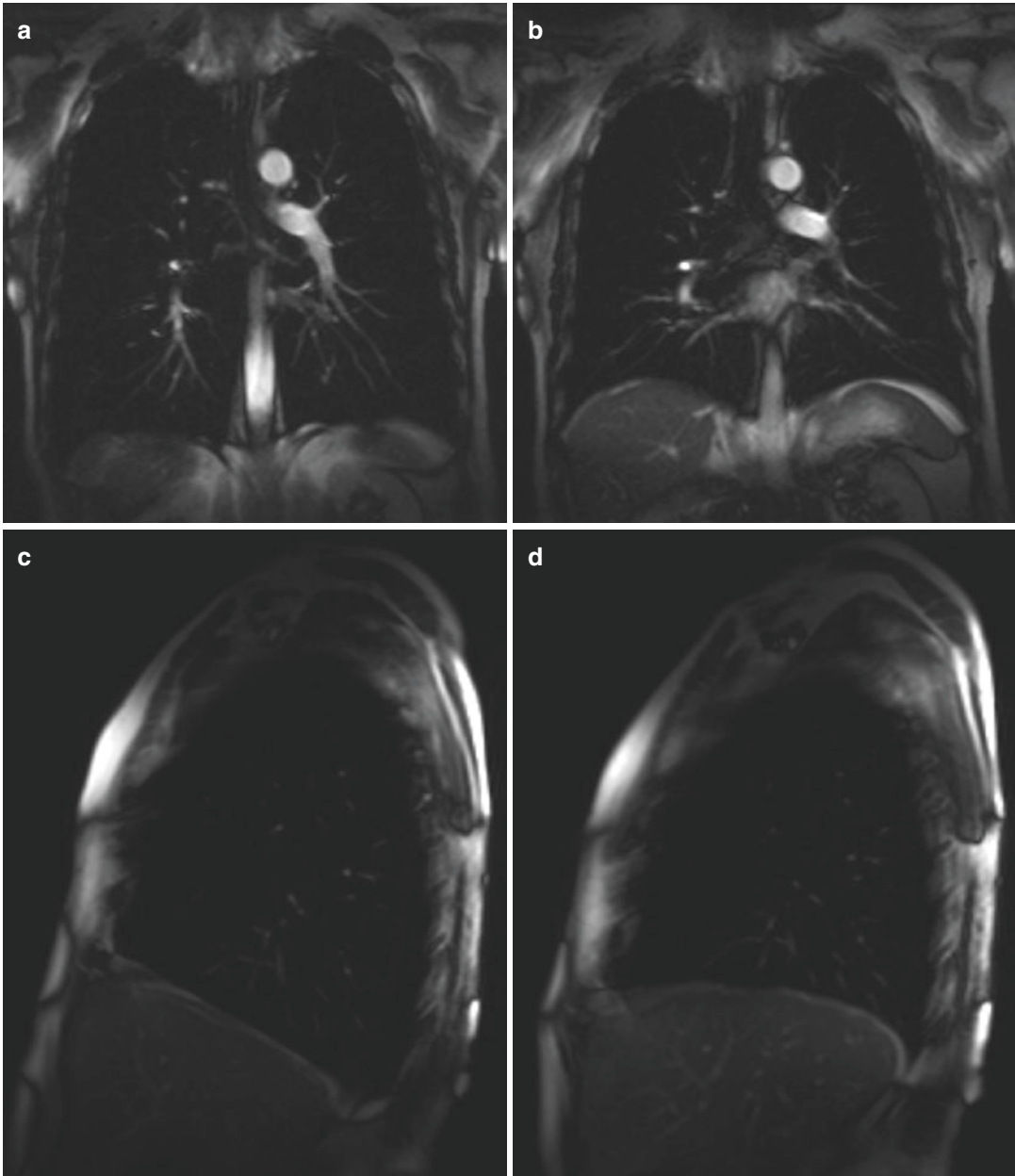
Fig. 4 Coronal and sagittal MR images taken from a dynamic series acquired in a COPD patient during forced expiration reflecting maximum inspiration (**a**, **c**) and maximum expiration (**b**, **d**) shows motion of the diaphragm and thoracic wall (*arrows*)

5.1 Oxygen-Enhanced Imaging

Oxygen-enhanced MRI does not require special scanner hardware and is easy to use and the overall material costs are low in comparison with noble gas imaging. The main idea behind this technique is to utilize the paramagnetic properties of inhaled oxygen (O_2) to obtain information regarding the pulmonary blood flow

volume and integrity of the lung parenchyma. Several investigators reported that oxygen-enhanced MRI could demonstrate regional ventilation (Edelman et al. 1996; Loffler et al. 2000; Ohno et al. 2001). Only few studies have successfully applied oxygen-enhanced MRI to patients with pulmonary diseases in a clinical setting. One of the reasons might be that the use of high oxygen concentrations (15 L/min) may not be without risk in patients with severe COPD and therefore vital parameters should be monitored during the procedure.

In some basic measurements it was shown that the T1 of the lung parenchyma is significantly shorter in patients with emphysema than in volunteers (Stadler et al. 2008). In a preliminary study an inhomogeneous and weak signal intensity increase after application of oxygen was observed, compared to healthy volunteers (Muller et al. 2002). Ohno et al. demonstrated that regional changes in ventilation as observed in oxygen-enhanced MR reflected regional lung function. The maximum mean relative enhancement ratio correlated with the diffusion capacity for carbon monoxide ($r^2 = 0.83$), while the mean slope of relative enhancement was strongly correlated with the FEV_1 ($r^2 = 0.74$) and the maximum mean relative enhancement with the high-resolution CT emphysema score ($r^2 = 0.38$) (Ohno et al. 2003). The simple administration of pure oxygen might induce the pulmonary arteries to dilate resulting in an increase of pulmonary blood volume and a consecutive increase in signal intensity (Ley et al. 2007).

This technique might be further refined by exploiting time-resolved acquisitions during oxygen wash-in and washout. Mean wash-in time showed good correlation with FEV1/FVC% and FEV1% ($r = -0.74$) and moderate correlation with DLCO% ($r = -0.57$) in a cohort of 10 non-smokers and 61 smokers without or with mild to severe COPD (Ohno et al. 2008a). Mean wash-in time was significantly different between non-smokers (smallest) and COPD patients at risk of or with mild COPD, while moderate and severe stages of the disease were significantly different to all other subgroups. In a larger study population of 160 smokers without and with mild to very

severe COPD, similar good correlation was found between mean relative enhancement ratio and FEV1/FVC% ($r = 0.68$), FEV1% ($r = 0.65$), and moderate correlation with DLCO% ($r = 0.61$), all slightly better than correlation coefficients between quantitative CT and pulmonary function tests (Ohno et al. 2008b). These results were confirmed in another study in 187 smokers (Ohno et al. 2012). Pulmonary functional parameters and mean relative enhancement ratio for each clinical subgroup showed significant differences among each other, thus suggesting that oxygen-enhanced MRI is effective for pulmonary functional loss assessment and clinical stage classification of smoking-related COPD.

The feasibility of oxygen-enhanced MRI to detect a response to a single-dose bronchodilator therapy as well as 8-week treatment with a combination of an inhaled corticosteroid and bronchodilator was tested in a recent study and demonstrated improvement of FEV1 and MRI ventilation parameters (Morgan et al. 2014).

5.2 Hyperpolarized Noble Gas Imaging

Over the past decade hyperpolarized noble gas MRI using [3]Helium and [129]Xenon was developed to improve imaging of pulmonary structure, ventilation, dynamics, and oxygen uptake (Ley-Zaporozhan and van Beek 2010). [3]Helium became the most widely used gas for these studies as it provides higher signal-to-noise ratios than [129]Xenon, due to its lower intrinsic gyromagnetic ratio, and its confinement to the airways and airspaces without dissolving into the surrounding tissue and bloodstream (van Beek et al. 2004). Areas with ventilation defects caused by airway obstruction and emphysema represent the only limitation because they cannot be assessed due to lack of the tracer gas entering these areas. Thus, there is almost no information about these affected lung regions. Overall, the intrinsic high cost of these noble gases, need for laser-induced hyperpolarization hardware, and need for non-proton imaging hardware and software remain the major drawbacks of this technology on its

way to broader clinical applications. The field of hyperpolarized noble gas imaging is currently undergoing some changes due to supply issues of [3]Helium, while development of [129]Xenon is increasingly encouraging due to novel polarizer systems that offer higher levels of polarization with resultant better signal (Ley-Zaporozhan and van Beek 2010).

5.2.1 Static Ventilation

Airflow obstruction leads to a reduced level of [3]Helium in the distal lung regions allowing for sensitive detection of ventilation abnormalities (Figs. 5 and 6) (Kauczor et al. 1996). In healthy smokers with normal lung function even subtle ventilation defects were visualized demonstrating the high sensitivity of the technique (Guenther et al. 2000). Ventilation defects correlated well with the parenchymal destruction assessed by HRCT in patients with severe emphysema following single-lung transplantation (Gast et al. 2002). To date, the largest multicenter trial was performed in three European centers analyzing 94 subjects with COPD, α1-antitrypsin-deficiency patients, and healthy age-matched never-smokers (van Beek et al. 2009). The visually estimated non-ventilated lung volumes on [3]He-MRI were compared to percentage of diseased lung on HRCT. Using PFT as a reference, regional analysis of [3]He-MRI and HRCT correctly categorized normal volunteers in 100% and 97%, COPD in 42% and 69%, and α1-antitrypsin-deficiency patients in 69% and 85% of cases, respectively. Overall only a moderate agreement (kappa = 0.43) was found between [3]He-MRI and HRCT. Direct comparison revealed that 23% of subjects with moderate/severe structural abnormalities had only mild ventilation defects.
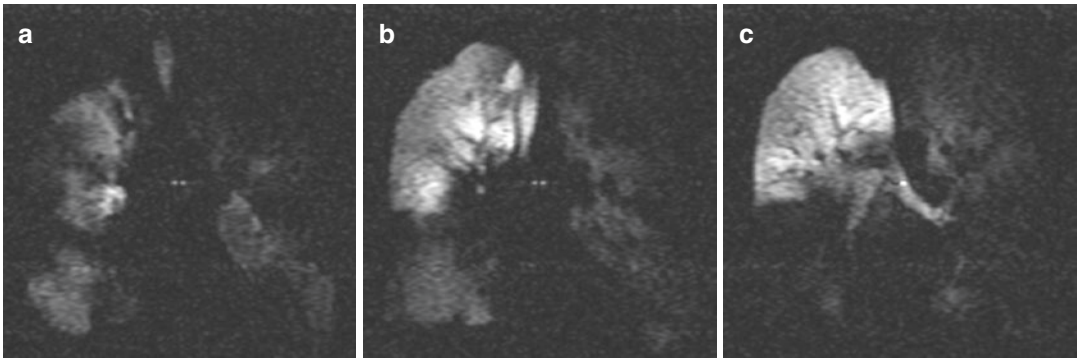

Fig. 5 MR ventilation images using hyperpolarized [3]Helium gas of a patient suffering from alpha1-antitrypsin deficiency: good ventilation of the right upper lobe and large wedge-shaped ventilation defects in all remaining lung areas
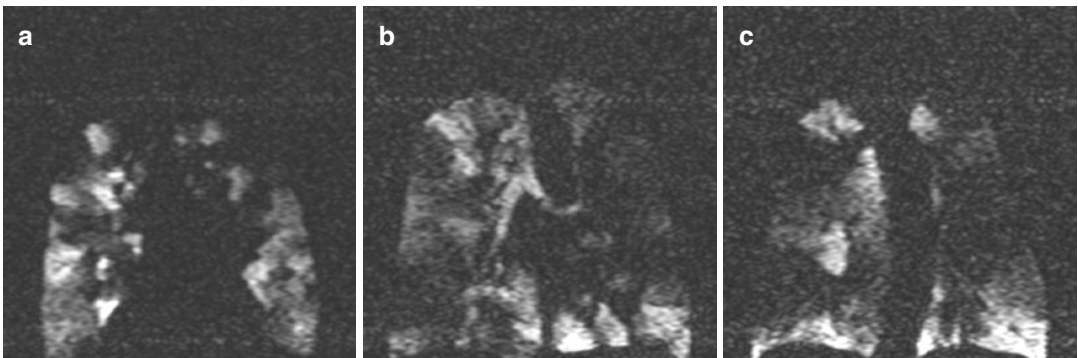

Fig. 6 MR ventilation images using hyperpolarized [3]Helium gas of a patient suffering from COPD: focal and wedge-shaped ventilation defects in all parts of the lung

The most common metric used in the early literature was the mean number of ventilation defects per slice without information about the size and regional distribution of the defect (Fain et al. 2010). By use of estimated lung boundaries the volume of ventilated lung areas on ³He-MRI correlated well with vital capacity ($r = 0.9$) and the amount of non-emphysematous volume on CT ($r = 0.7$) in patients with severe emphysema following single-lung transplantation (Zaporozhan et al. 2004). Today an established approach is to calculate the ventilated lung volume and normalize it to total lung volume, resulting in percentage of lung volume ventilated or its derivate percentage volume of defect. These values are quantified by semiautomated segmentation of ³He ventilation images and further registration to proton MR images for delineation of the lungs and defect boundaries. Repeatability and validity of this measure were shown in several studies in several disease entities (Kruger et al. 2016). Using this approach in small-scale studies, a good correlation between ventilation defect percentage and $FEV_1\%$ and FEV_1/FVC was found by Kirby et al. ($r = -0.84$) (Kirby et al. 2012a) but only fair correlation by Mathew et al. ($r = -0.58$ and -0.54, respectively) (Mathew et al. 2011). Even more reproducible quantification of percentage ventilation volume could be achieved by acquiring ³He ventilation images and anatomical proton images during the same single breath-hold (Horn et al. 2014).

The voxel intensity of the ventilation images can be further classified into clusters representing graduations of signal intensity from no signal, hypointense signal to hyperintense signal, and generating ventilation cluster maps (Kirby et al. 2011). This in-depth distribution analysis might be of value for therapy monitoring. Advantages of this evaluation were shown in a small-scale study of patients with moderate to severe COPD, where ³He-MRI depicted significant improvements in the regional gas distribution throughout the lung after bronchodilator therapy with and without clinically important changes in FEV_1 (Kirby et al. 2011). In a 2-year longitudinal study in patients with mild to moderate COPD, ventilation defect percentage worsened significantly in the absence of significant decline in FEV1, suggesting sensitivity of ³He-MRI for depicting disease progression (Kirby et al. 2010).

Given its greater availability and lower cost, ¹²⁹Xenon offers an alternative to ³He-MRI. The associated lower signal-to-nose ratio of ¹²⁹Xenon images requires careful segmentation of the lung from background noise (Kaushik et al. 2011). The gas distribution at ¹²⁹Xe-MRI was qualitatively more regionally heterogeneous and the ventilation defect percentage was significantly greater than that with ³He-MRI in patients with COPD but not in healthy volunteers, suggesting incomplete or delayed filling of lung regions (Kirby et al. 2012a). Lower diffusion coefficient and higher viscosity of xenon relative to helium may result in slower gas movement and filling into distal diseased lung regions. The ventilation defect percentage from ¹²⁹Xe-MRI showed a good correlation with $FEV_1\%$ and FEV_1/FVC in a small group of COPD patients and age-matched controls ($r = -0.79$ and $r = -0.71$, respectively) and also in a small group of COPD patients and healthy volunteers ($r = -0.89$ and $r = -0.95$, respectively) (Kirby et al. 2012a; Virgincar et al. 2013).

5.2.2 Dynamic

³He-MR imaging with high temporal resolution via ultrafast echo-planar (EPI), gradient-echo, and interleaved spiral sequences allows for the visualization and assessment of the various inspiratory and expiratory phases of respiration. The instantaneous visualization of the bolus movement leads to a direct evaluation of the regional distribution of ventilation throughout the lungs, which may be quantified using a regional assessment (Lehmann et al. 2004). Evaluation of the overall usefulness of the technique has shown considerable airflow abnormalities in diseased lung states and normal respiration stages in normal lungs (Salerno et al. 2001; Wild et al. 2003). Normal respiration can be described by a rapid and homogenous distribution of the gas throughout the lung, whereas in diseased lungs, the airflow is inhomogeneous due to factors such as airway blockages and reduced lung compliance, leading to interspersed ventilation defects (Fig. 7). The observed ventilation defects vary
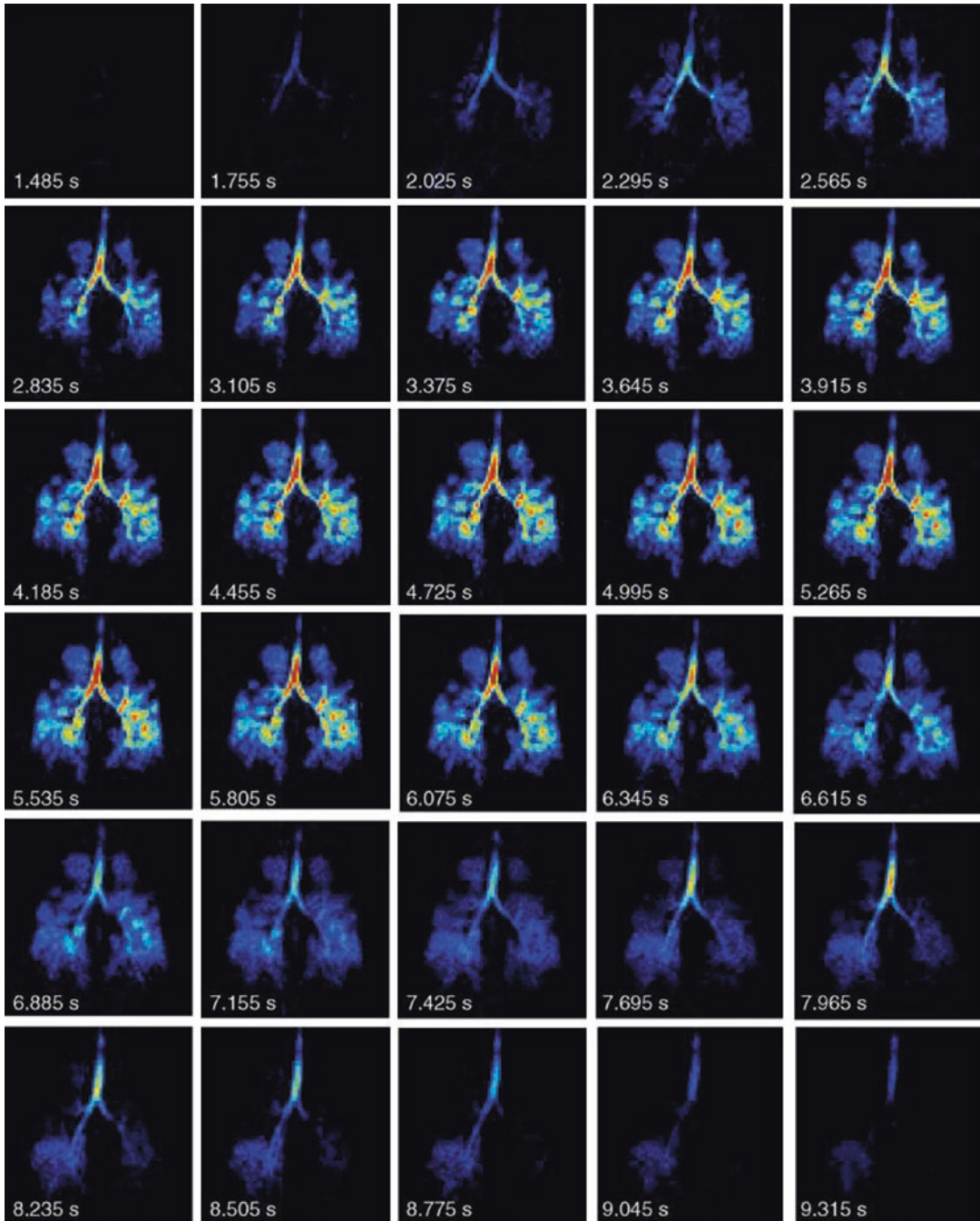
Fig. 7 Dynamic MR ventilation images using hyperpolarized ³Helium gas from a COPD patient showing regions of ventilation obstruction in both lungs, particularly in the upper lobes, and a delayed emptying/depolarization of gas in the lower left lobe, which could be indicative of air trapping. Reprinted with permission from van Beek et al. (2004)

from reduced inflow to air trapping as observed in the later phases of the respiratory cycle, which are more markedly visualized in subjects with CT-proven centrilobular emphysema (Wild et al. 2003; Gierada et al. 2000; Gast et al. 2003).

Another recently used approach was to evaluate delayed ventilation during the time course of breath-hold imaging by using time-resolved gradient-echo sequence with 3D whole-lung coverage (Marshall et al. 2012). The influx of polarized gas into initially non-ventilated defects might represent collateral ventilation and slow filling of peripheral airspaces due to increased flow resistance. Delayed filling was observed in eight of ten COPD patients.

5.2.3 ^{3}Helium Apparent Diffusion Coefficient (ADC)

The high diffusion coefficient of ^{3}Helium gas makes it very suitable for the evaluation of the lung microstructure, connecting pores and pathways, leading to an overall assessment of the integrity and size of such structures. The ADC is a reflection of the restricted diffusion of ^{3}Helium gas in a normal airway system due to the relatively small size of airways in relation to the diffusivity of the gas.

Similar to all other ^{3}Helium techniques, the ADC is accomplished throughout one single breath-hold, where a series of images are acquired and evaluated on a pixel-by-pixel basis. The introduction of the additional gradients into the sequences allows the monitoring of diffusion through signal decay incurred by motion of the helium molecules, thus creating a map of diffusion values representing the regional and global integrity of the lungs.

ADC maps of normal healthy volunteers have shown to be homogenous and uniform. On the other hand, in emphysematous subjects ADC maps were nonuniform and contained larger diffusion values. This nonuniformity of the ADC values correlates well with the nature of the disease, where the degree and location of destruction vary throughout the lung (Salerno et al. 2002; Ley et al. 2004a; Conradi et al. 2005). The ability to distinguish between normal and emphysematous lungs reflects the overall power

of determining and quantifying airway enlargement along with tissue destruction. The mean ADC for emphysema patients (0.452 cm^2/s) was found to be significantly larger ($p < 0.002$) than for normal volunteers (0.225 cm^2/s) (Salerno et al. 2002). In other studies, mean ADC values of emphysema patients were as low as 0.24 cm^2/s and as high as 0.55 cm^2/s (Conradi et al. 2005; Swift et al. 2005; Diaz et al. 2009). This wide distribution of ADC values for the emphysema population can be attributed to the variability in airspace size and morphological alterations of the distal airspaces caused by the disease. Values for ^{129}Xe-ADC are lower than ^{3}He-ADC by an order of magnitude due to higher density of xenon gas (Kruger et al. 2016). ^{129}Xe-ADC for emphysema patients (0.056 cm^2/s) was significantly different than for age-matched controls (0.043 cm^2/s) and for healthy volunteers (0.036 cm^2/s) (Kaushik et al. 2011).

Very high reproducibility of these ADC measures has been demonstrated—within 6% variation for consecutive scans at the same day (Morbach et al. 2005) and in another study with a correlation of $r^2 > 0.9$ for re-scanning on the same day as well as in a week interval (Mathew et al. 2008). In a small study combining ^{3}He and ^{129}Xe imaging in ten patients, mean ^{3}He-ADC within the regions only assessed by helium gas was significantly greater than for lung regions assessed by both gases (0.503 cm^2/s versus 0.470 cm^2/s) (Kirby et al. 2013). ^{3}He-ADC values showed a moderate correlation with FEV$_1$% ($r = -0.6$) (Swift et al. 2005) and good correlation with DLCO% ($r = -0.82$) (Diaz et al. 2009). ^{129}Xe-ADC showed good to moderate correlation with FEV$_1$%, FEV1/FVC%, and DLCO% in COPD patients and age-matched controls ($r = -0.77$) (Kaushik et al. 2011) as well as in COPD and healthy volunteers ($r = -0.67$, $r = -0.77$ and $r = -0.79$, respectively) (Kirby et al. 2012a).

Mean ADC probably underestimates the amount of destroyed lung tissue, as ventilation defects prevent ADC measurements, and some of the most destroyed emphysematous lung areas therefore are excluded from the analysis.

In a small study investigating ^{3}He-ADC before and after bronchodilator administration a signifi-

cant decrease in ADC value was detected within the lung regions containing the ³He signal at both time points (Kirby et al. 2012b). No difference was found between ventilated areas before bronchodilator administration and newly ventilated lung regions after the bronchodilator administration, suggesting that these regions have a similar degree of the disease.

6   Pulmonary Perfusion

Perfusion and ventilation are normally in balance, with hypoxic vasoconstrictive response providing a method to optimize lung function. In patients with COPD, ventilation is impaired due to airway obstruction and parenchymal destruction, leading to perfusion being moved to better ventilated lung regions or shunting of blood (moving through the lungs without reaching a capillary bed for gas exchange) (Moonen et al. 2005). The reduction of the pulmonary vascular bed is related to the severity of parenchymal destruction (Thabut et al. 2005); however the distribution of perfusion does not necessarily match parenchymal destruction (Sandek et al. 2002; Ley-Zaporozhan et al. 2007). Conventional radionuclide perfusion scintigraphy has been used to assess these abnormalities, but it has substantial limitations with respect to spatial and temporal resolution. A superior technique is SPECT, which is rarely used as it is rather time consuming and not routinely applied. Inflammation appears to play a critical role in the maintenance of the hypoxic vasoconstrictive response, and PET studies with endotoxin challenge have shown that this response is shut off when inflammation and lung injury occur (Schuster and Marklin 1986; Gust et al. 1998).

The basic principle of contrast-enhanced perfusion MRI is a dynamic acquisition during and after an intravenous bolus injection of a paramagnetic contrast agent. With the introduction of parallel imaging techniques, 3D perfusion imaging with a high spatial and temporal resolution as well as an improved anatomical coverage and z-axis resolution can be acquired (Ley et al. 2004b; Fink et al. 2004, 2005). These data sets are also well suited for high-quality multiplanar reformats. Due to high spatial resolution, detailed analysis of pulmonary perfusion and precise anatomical localization of the perfusion defects on a lobar and even segmental level can be performed (Fig. 8). Quantitative values for pulmonary perfusion can be obtained by applying the principles of indicator dilution techniques. The quantitative indices, such as mean transit time (MTT), pulmonary blood volume (PBV), and blood flow (PBF), are derived from the time intensity curve, defined by the dynamic series of perfusion MR images.

MR perfusion allows for a high diagnostic accuracy in detecting perfusion abnormalities (Fink et al. 2004; Sergiacomi et al. 2003). Furthermore, MR perfusion ratios correlate well with radionuclide perfusion scintigraphy ratios (Ohno et al. 2004a; Molinari et al. 2006). Lobar and segmental analysis of the perfusion defects can be achieved. In patients with severe emphy-
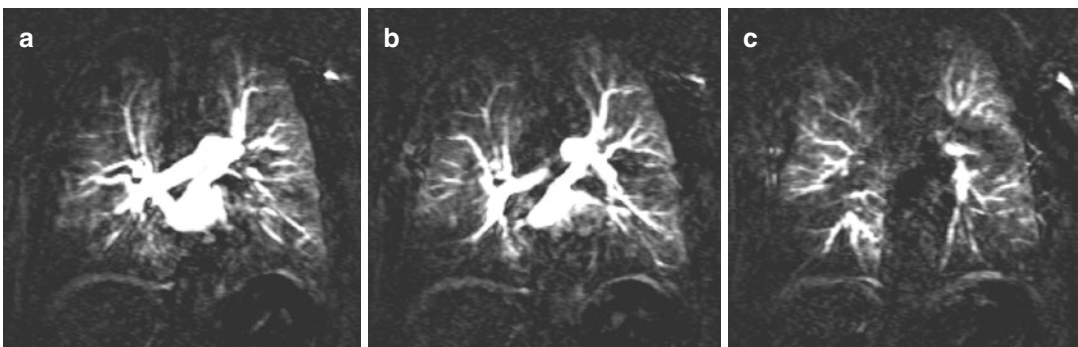

Fig. 8 Coronal contrast-enhanced MR perfusion images of a COPD patient acquired during an inspiratory breath-hold showing subpleural distribution of perfusion defects

sema there was a strong match between parenchymal destruction and reduction of perfusion; however the distribution patterns of emphysema and perfusion impairment were not necessarily in concordance (Ley-Zaporozhan et al. 2007). Here the severity score was higher on CT in 16% of the lobes and on MRI in 5%. In otherwise healthy smokers there were more MR perfusion defects than parenchymal abnormalities seen on CT, suggesting MR perfusion being a good approach to identify early evidence of COPD (Fan et al. 2013).

The perfusion abnormalities in COPD clearly differ from those caused by vascular obstruction. While wedge-shaped perfusion defects occur in embolic vascular obstruction, a low degree of contrast enhancement is generally found in patients with COPD/emphysema (Amundsen et al. 2002; Morino et al. 2006). Furthermore, the peak signal intensity is usually reduced. These features allow for easy visual differentiation. In patients with COPD, the quantitative evaluation of 3D perfusion showed that the mean PBF, PBV, and MTT were significantly decreased, and these changes showed a very heterogeneous distribution (Ohno et al. 2004b). It was discussed that patients with emphysema have hypoxia as well as destruction of lung parenchyma and fewer alveolar capillaries. This causes increased pulmonary arterial resistance and, secondarily to adaptive processes, pulmonary hypertension and right ventricular dysfunction. Ultimately, this results in decreased pulmonary blood flow in addition to heterogeneous perfusion and decreased PBV. MTT is determined by the ratio between PBV and PBF. The results suggested that MTT is significantly decreased, reflecting a larger degree of decrease in PBV compared with PBF, with concomitant increased heterogeneity of regional PBV. Obviously, accurate quantitative measurements of such regional changes are important for improved understanding of lung pathophysiology in COPD.

For visual assessment of the regional heterogeneity the area of perfusion impairment on color-coded maps covering 10–15 cm of the thorax was compared with the same area of emphysema on quantitative CT maps. Very good or good agreement was found in 9–10 of 14 patients (two readers) for PBF and in 11/14 patients (similar for both readers) for PBV (Jang et al. 2008). The quantitative evaluation was performed in small peripheral ROIs on each slice for upper, middle, and lower areas of the lung. Here only moderate correlation was found between PBV and emphysema fraction on volumetric CT ($r = -0.61$) and FEV1/FVC ($r = 0.69$).

An association between the emphysema type on CT and MR perfusion pattern was analyzed at a segmental level in patients with severe emphysema (Bryant et al. 2015). The centrilobular type of emphysema showed corresponding heterogeneous perfusion with focal defects in 70% (Fig. 9a), whereas panlobular emphysema presented with either homogeneous or heterogeneous absence of perfusion in 42% and 43%, respectively (Fig. 9b, c).

The repeatability and reproducibility of quantitative whole-lung perfusion in inspiration and expiration were analyzed in healthy volunteers by two observers (Ley-Zaporozhan et al. 2011). The intraobserver differences between the initial examination and follow-up after 24 h were not significantly different for PBV, MTT, and TTP for both observers. However, PBF showed a sig-

Fig. 9 (**a**) For the segments of the middle and lower lobes centrilobular emphysema was found to be the predominant type on CT, corresponding color-coded map of max. Peak enhancement of MR perfusion showed heterogeneous perfusion with defects as the predominant pattern. (**b**) The apical segment of both lungs showed centrilobular emphysema as the predominant type on CT (*arrows*), corresponding color-coded map of max. Peak enhancement of MR perfusion showed heterogeneous loss of perfusion as the predominant pattern. (**c**) For the segments of both lower lobes panlobular emphysema was found to be the predominant type on CT (*arrows*), corresponding color-coded map of max. Peak enhancement of MR perfusion showed homogeneous loss of perfusion as the predominant pattern (*arrows*). Reprinted with permission from Bryant et al. (2015)
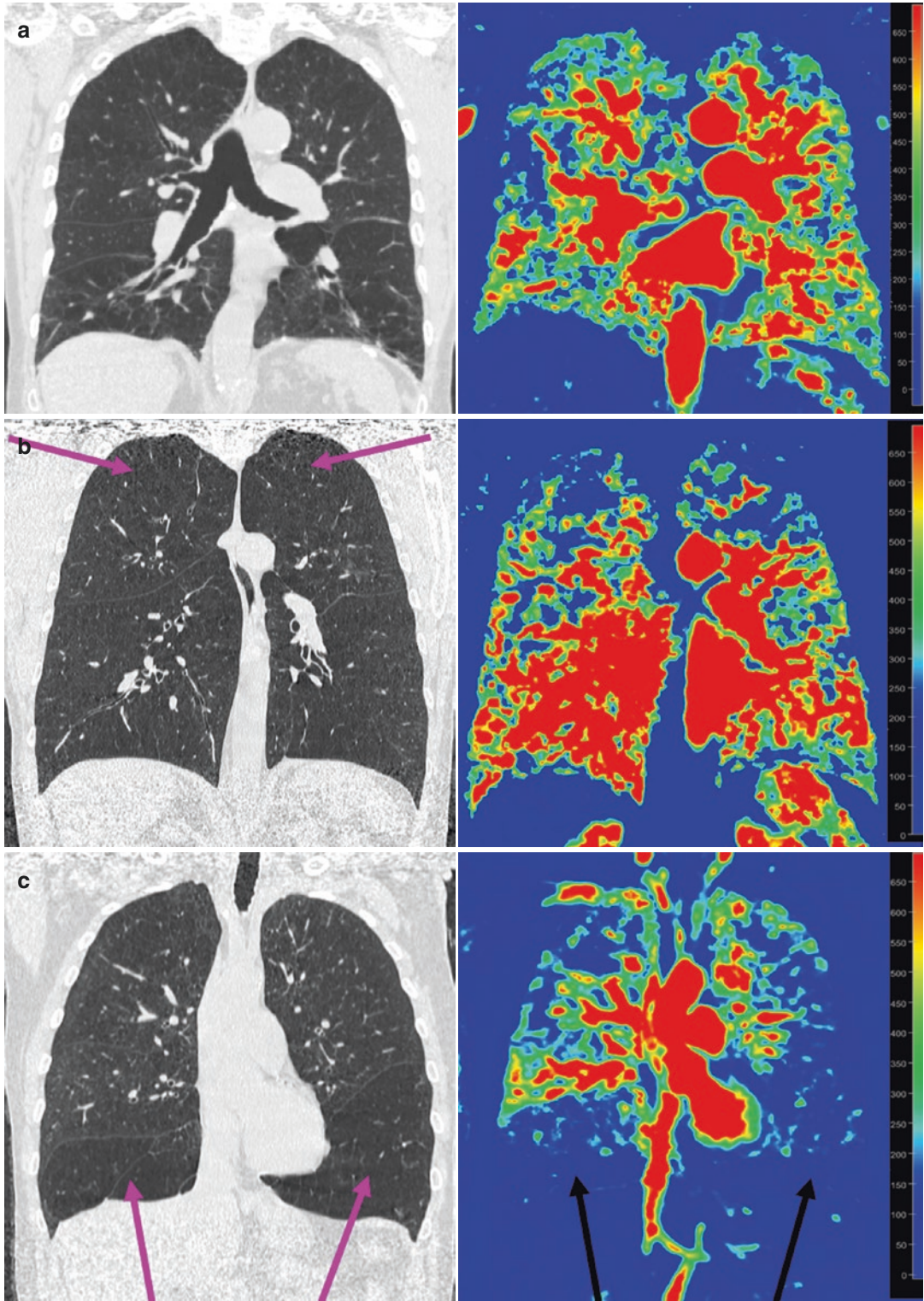
nificant difference for both observers but only on inspiration. For interobserver evaluation, all parameters except inspiratory PBF were significantly different ($P < 0.0001$). Thus, the quantitative perfusion MRI showed reproducible results, but the evaluation is highly dependent on the observer and the quantitative analysis of the serial examinations should be performed by the same person.

In the largest study to date, the quantitative perfusion parameters were markedly reduced in mild COPD as well as in more severe stages compared to healthy smokers; however evaluation was limited to one coronal slice (Hueper et al. 2015). Thus, there is a need for fast, dedicated post-processing software for whole-lung assessment, which is especially necessary in longitudinal studies or screening trials for further investigation of perfusion as a possible imaging biomarker. A fully automatic method was recently introduced by Kohlmann et al. (2015). Similar to ventilation imaging, the lungs were segmented on the morphological MR images with higher spatial resolution and the segmentation was then transferred to the perfusion images via nonlinear registration. The automatic segmentation took approximately 1 min and no user interaction was required, whereas the time for the manual segmentation ranged between 12 and 25 min. The reproducibility of the quantitative

analysis may also be improved by using automatic instead of manual lung segmentation.

In a recent study evaluating perfusion during acute exacerbation of COPD, two patient groups were identified—one presented with an improvement of quantitative perfusion parameters after clinical stabilization and another showed no response (Sergiacomi et al. 2014). This could assist in predicting early response to treatment, allowing more aggressive approaches in nonresponders.

7 Hemodynamics

Assessment of right ventricular function is important, as this is where the strain of perfusion obstruction and pulmonary hypertension eventually leads to the demise of the patient. MRI is able to assess right ventricular function through either phase-contrast flow measurements in the pulmonary trunk (Fig. 10) or short-axis cine acquisition of the right ventricle (Vonk-Noordegraaf et al. 2005; Gatehouse et al. 2005). Thus, early changes of the complex geometry of the right ventricular wall and chamber volume can be accurately measured.

Although pulmonary hypertension and cor pulmonale are rather common sequelae of COPD, the direct mechanism remains unclear (Szilasi
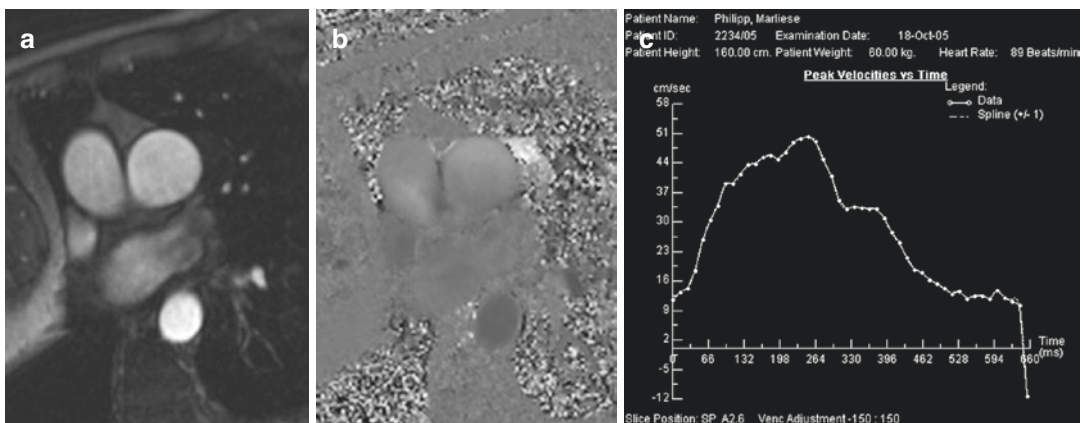

Fig. 10 Quantitative flow measurement of pulmonary blood flow. Magnitude (**a**) and velocity-encoded (**b**) image of the pulmonary trunk (*arrow*). Results of peak velocity over time (**c**) show the prolonged increase of velocity at the beginning of the systolic phase followed by an abnormal plateau during diastole

et al. 2006). In COPD patients the pulmonary vessels show a reduced capacity for vessel dilatation due to a defect in synthesis and/or release of nitric oxide. Prior to the onset of clinical symptoms patients exhibit signs of vascular bed obstruction and elevated pulmonary artery pressure including main pulmonary artery dilatation. Pulmonary hypertension is most often mild to moderate (mean pulmonary artery pressure in the range of 20–35 mm Hg), but it may worsen markedly during acute exacerbations, sleep, and exercise. Assessment of the pulmonary arterial pressure is necessary in COPD patients for at least two reasons: such patients have a poor prognosis; and they need adequate treatment that might include pulmonary vasodilators.

It has been demonstrated by several studies that the level of pulmonary hypertension has a prognostic impact on COPD patients. In one of these studies, the 5-year survival rates were 50% in patients with mild (20–30 mm Hg), 30% in those with moderate to severe (30–50 mm Hg), and 0% in the small group ($n = 15$) of patients with very severe pulmonary hypertension (>50 mm Hg). Thus, severe pulmonary hypertension carries a poor prognosis, and this has also been observed in COPD patients receiving long-term oxygen therapy (Weitzenblum and Chaouat 2005).

Initially, a rise in pulmonary blood pressure leads to pulmonary artery dilatation while right ventricular performance is usually maintained. Evaluation of the right ventricle and pulmonary blood flow by echocardiography is difficult in patients with emphysema as the acoustic window is limited. Therefore, MRI has been used for imaging the right ventricle, and a loose correlation between increased right ventricular mass and severity of emphysema was demonstrated (Boxt 1996).

In COPD patients with hypoxemia, increased right ventricular volumes, decreased right ventricular function, and impaired left ventricular diastolic function were shown (Budev et al. 2003). In a study by Vonk-Nordegraaf et al. the right ventricular mass and ejection fraction in 25 clinically stable, normoxic COPD patients

with emphysema were analyzed. The position of the heart appeared rotated and shifted to a more vertical position in the thoracic cavity due to hyperinflation of the lungs with an increase of the retrosternal space. The right ventricular wall mass was significantly higher (68 g) in the patient group compared to healthy volunteers (59 g). The right ventricular ejection fraction was unchanged (53%) (Vonk Noordegraaf et al. 1997). In another study from the same group structural and functional cardiac changes in COPD patients with normal P_aO_2 and without signs of right ventricular failure were evaluated. Compared to healthy volunteers there were no indications of pulmonary hypertension. However, the end-systolic and end-diastolic volumes of the right ventricle were significantly reduced (with normal ejection fraction), the right ventricular mass was significantly elevated while the left ventricular mass was within normal limits. The authors conclude that concentric right ventricular hypertrophy is the earliest sign of right ventricular pressure increase in patients with COPD. This structural adaptation of the heart initially does not alter right and left ventricular systolic function (Vonk-Noordegraaf et al. 2005). As this is the only study so far in patients with mild emphysema no strong conclusions can be drawn from this first description of the early adaptation mechanisms of the right ventricle in patients with normoxemia or mild hypoxemia and the consequences of any structural changes on right and left ventricular function.

References

Alamidi DF, Morgan AR, Hubbard Cristinacce PL, Nordenmark LH, Hockings PD, Lagerstrand KM et al (2016) COPD patients have short lung magnetic resonance T1 relaxation time. COPD 13(2):153–159. doi: 10.3109/15412555.2015.1048851

Amundsen T, Torheim G, Kvistad KA, Waage A, Bjermer L, Nordlid KK et al (2002) Perfusion abnormalities in pulmonary embolism studied with perfusion MRI and ventilation-perfusion scintigraphy: an intra-modality and inter-modality agreement study. J Magn Reson Imaging 15(4):386–394

Bankier AA, O'Donnell CR, Mai VM, Storey P, De Maertelaer V, Edelman RR et al (2004) Impact of lung volume on MR signal intensity changes of the lung parenchyma. J Magn Reson Imaging 20(6):961–966

Bauman G, Scholz A, Rivoire J, Terekhov M, Friedrich J, de Oliveira A et al (2013) Lung ventilation- and perfusion-weighted Fourier decomposition magnetic resonance imaging: in vivo validation with hyperpolarized 3He and dynamic contrast-enhanced MRI. Magn Reson Med 69(1):229–237. doi:10.1002/mrm.24236

van Beek EJ, Wild JM, Kauczor HU, Schreiber W, Mugler JP III, de Lange EE (2004) Functional MRI of the lung using hyperpolarized 3-helium gas. J Magn Reson Imaging 20(4):540–554

van Beek EJ, Dahmen AM, Stavngaard T, Gast KK, Heussel CP, Krummenauer F et al (2009) Hyperpolarised 3He MRI versus HRCT in COPD and normal volunteers: PHIL trial. Eur Respir J 34(6):1311–1321. doi:10.1183/09031936.00138508

Biederer J, Both M, Graessner J, Liess C, Jakob P, Reuter M et al (2003) Lung morphology: fast MR imaging assessment with a volumetric interpolated breath-hold technique: initial experience with patients. Radiology 226(1):242–249

Boxt LM (1996) MR imaging of pulmonary hypertension and right ventricular dysfunction. Magn Reson Imaging Clin N Am 4(2):307–325

Bryant M, Ley S, Eberhardt R, Menezes R, Herth F, Sedlaczek O et al (2015) Assessment of the relationship between morphological emphysema phenotype and corresponding pulmonary perfusion pattern on a segmental level. Eur Radiol 25(1):72–80. doi:10.1007/s00330-014-3385-5

Budev MM, Arroliga AC, Wiedemann HP, Matthay RA (2003) Cor pulmonale: an overview. Semin Respir Crit Care Med 24(3):233–244

Cluzel P, Similowski T, Chartrand-Lefebvre C, Zelter M, Derenne JP, Grenier PA (2000) Diaphragm and chest wall: assessment of the inspiratory pump with MR imaging-preliminary observations. Radiology 215(2):574–583

Conradi MS, Yablonskiy DA, Woods JC, Gierada DS, Jacob RE, Chang YV et al (2005) 3He diffusion MRI of the lung. Acad Radiol 12(11):1406–1413

Coxson HO, Leipsic J, Parraga G, Sin DD (2014) Using pulmonary imaging to move chronic obstructive pulmonary disease beyond FEV1. Am J Respir Crit Care med 190(2):135–144. doi:10.1164/rccm.201402-0256PP

Decramer M (1997) Hyperinflation and respiratory muscle interaction. Eur Respir J 10(4):934–941

Diaz S, Casselbrant I, Piitulainen E, Magnusson P, Peterson B, Wollmer P et al (2009) Validity of apparent diffusion coefficient hyperpolarized 3He-MRI using MSCT and pulmonary function tests as references. Eur J Radiol 71(2):257–263. doi:10.1016/j.ejrad.2008.04.013

Edelman RR, Hatabu H, Tadamura E, Li W, Prasad PV (1996) Noninvasive assessment of regional ventilation in the human lung using oxygen-enhanced magnetic resonance imaging. Nat Med 2(11):1236–1239

Eichinger M, Tetzlaff R, Puderbach M, Woodhouse N, Kauczor HU (2007) Proton magnetic resonance imaging for assessment of lung function and respiratory dynamics. Eur J Radiol 64(3):329–334

Fain S, Schiebler ML, McCormack DG, Parraga G (2010) Imaging of lung function using hyperpolarized helium-3 magnetic resonance imaging: review of current and emerging translational methods and applications. J Magn Reson Imaging 32(6):1398–1408. doi:10.1002/jmri.22375

Fan L, Xia Y, Guan Y, Yu H, Zhang TF, Liu SY et al (2013) Capability of differentiating smokers with normal pulmonary function from COPD patients: a comparison of CT pulmonary volume analysis and MR perfusion imaging. Eur Radiol 23(5):1234–1241. doi:10.1007/s00330-012-2729-2

Fink C, Puderbach M, Bock M, Lodemann KP, Zuna I, Schmahl A et al (2004) Regional lung perfusion: assessment with partially parallel three-dimensional MR imaging. Radiology 231(1):175–184

Fink C, Ley S, Kroeker R, Requardt M, Kauczor HU, Bock M (2005) Time-resolved contrast-enhanced three-dimensional magnetic resonance angiography of the chest: combination of parallel imaging with view sharing (TREAT). Investig Radiol 40(1):40–48

Gast KK, Viallon M, Eberle B, Lill J, Puderbach MU, Hanke AT et al (2002) MRI in lung transplant recipients using hyperpolarized (3)He: comparison with CT. J Magn Reson Imaging 15(3):268–274

Gast KK, Puderbach MU, Rodriguez I, Eberle B, Markstaller K, Knitz F et al (2003) Distribution of ventilation in lung transplant recipients: evaluation by dynamic 3He-MRI with lung motion correction. Investig Radiol 38(6):341–348

Gatehouse PD, Keegan J, Crowe LA, Masood S, Mohiaddin RH, Kreitner KF et al (2005) Applications of phase-contrast flow and velocity imaging in cardiovascular MRI. Eur Radiol 15(10):2172–2184

Gierada DS, Saam B, Yablonskiy D, Cooper JD, Lefrak SS, Conradi MS (2000) Dynamic echo planar MR imaging of lung ventilation with hyperpolarized (3)He in normal subjects and patients with severe emphysema. NMR Biomed 13(4):176–181

Guenther D, Eberle B, Hast J, Lill J, Markstaller K, Puderbach M et al (2000) (3)He MRI in healthy volunteers: preliminary correlation with smoking history and lung volumes. NMR Biomed 13(4):182–189

Gust R, Kozlowski J, Stephenson AH, Schuster DP (1998) Synergistic hemodynamic effects of low-dose endotoxin and acute lung injury. Am J Respir Crit Care Med 157(6 Pt 1):1919–1926

Henderson AC, Ingenito EP, Salcedo ES, Moy ML, Reilly JJ, Lutchen KR (2007) Dynamic lung mechanics in late-stage emphysema before and after lung volume reduction surgery. Respir Physiol Neurobiol 155(3):234–242

Heussel CP, Ley S, Biedermann A, Rist A, Gast KK, Schreiber WG et al (2004) Respiratory lumenal change of the pharynx and trachea in normal subjects and COPD patients: assessment by cine-MRI. Eur Radiol 14(12):2188–2197

Hoffman EA, Lynch DA, Barr RG, van Beek EJ, Parraga G (2016) Pulmonary CT and MRI phenotypes that help explain chronic pulmonary obstruction disease pathophysiology and outcomes. J Magn Reson Imaging 43(3):544–557. doi:10.1002/jmri.25010

Hogg JC, Chu F, Utokaparch S, Woods R, Elliott WM, Buzatu L et al (2004) The nature of small-airway obstruction in chronic obstructive pulmonary disease. N Engl J Med 350(26):2645–2653

Horn FC, Tahir BA, Stewart NJ, Collier GJ, Norquay G, Leung G et al (2014) Lung ventilation volumetry with same-breath acquisition of hyperpolarized gas and proton MRI. NMR Biomed 27(12):1461–1467. doi:10.1002/nbm.3187

Hueper K, Vogel-Claussen J, Parikh MA, Austin JH, Bluemke DA, Carr J et al (2015) Pulmonary microvascular blood flow in mild chronic obstructive pulmonary disease and emphysema. The MESA COPD study. Am J Respir Crit Care Med 192(5):570–580. doi:10.1164/rccm.201411-2120OC

Iwasawa T, Yoshiike Y, Saito K, Kagei S, Gotoh T, Matsubara S (2000) Paradoxical motion of the hemidiaphragm in patients with emphysema. J Thorac Imaging 15(3):191–195

Iwasawa T, Kagei S, Gotoh T, Yoshiike Y, Matsushita K, Kurihara H et al (2002) Magnetic resonance analysis of abnormal diaphragmatic motion in patients with emphysema. Eur Respir J 19(2):225–231

Iwasawa T, Takahashi H, Ogura T, Asakura A, Gotoh T, Kagei S et al (2007) Correlation of lung parenchymal MR signal intensity with pulmonary function tests and quantitative computed tomography (CT) evaluation: a pilot study. J Magn Reson Imaging 26(6):1530–1536

Iwasawa T, Takahashi H, Ogura T, Asakura A, Gotoh T, Shibata H et al (2011) Influence of the distribution of emphysema on diaphragmatic motion in patients with chronic obstructive pulmonary disease. Jpn J Radiol 29(4):256–264. doi:10.1007/s11604-010-0552-8

Jang YM, Oh YM, Seo JB, Kim N, Chae EJ, Lee YK et al (2008) Quantitatively assessed dynamic contrast-enhanced magnetic resonance imaging in patients with chronic obstructive pulmonary disease: correlation of perfusion parameters with pulmonary function test and quantitative computed tomography. Investig Radiol 43(6):403–410. doi:10.1097/RLI.0b013e31816901ab

Jobst BJ, Wielputz MO, Triphan SM, Anjorin A, Ley-Zaporozhan J, Kauczor HU et al (2015a) Morpho-functional 1H-MRI of the lung in COPD: short-term test-retest reliability. PLoS One 10(9):e0137282. doi:10.1371/journal.pone.0137282

Jobst BJ, Triphan SM, Sedlaczek O, Anjorin A, Kauczor HU, Biederer J et al (2015b) Functional lung MRI in chronic obstructive pulmonary disease: comparison of T1 mapping, oxygen-enhanced T1 mapping

and dynamic contrast enhanced perfusion. PLoS One 10(3):e0121520. doi:10.1371/journal.pone.0121520

Kauczor HU, Hofmann D, Kreitner KF, Nilgens H, Surkau R, Heil W et al (1996) Normal and abnormal pulmonary ventilation: visualization at hyperpolarized He-3 MR imaging. Radiology 201(2):564–568

Kaushik SS, Cleveland ZI, Cofer GP, Metz G, Beaver D, Nouls J et al (2011) Diffusion-weighted hyperpolarized 129Xe MRI in healthy volunteers and subjects with chronic obstructive pulmonary disease. Magn Reson Med 65(4):1154–1165. doi:10.1002/mrm.22697

Kirby M, Mathew L, Wheatley A, Santyr GE, McCormack DG, Parraga G (2010) Chronic obstructive pulmonary disease: longitudinal hyperpolarized (3)He MR imaging. Radiology 256(1):280–289. doi:10.1148/radiol.10091937

Kirby M, Mathew L, Heydarian M, Etemad-Rezai R, McCormack DG, Parraga G (2011) Chronic obstructive pulmonary disease: quantification of bronchodilator effects by using hyperpolarized (3)He MR imaging. Radiology 261(1):283–292. doi:10.1148/radiol.11110403

Kirby M, Svenningsen S, Owrangi A, Wheatley A, Farag A, Ouriadov A et al (2012a) Hyperpolarized 3He and 129Xe MR imaging in healthy volunteers and patients with chronic obstructive pulmonary disease. Radiology 265(2):600–610. doi:10.1148/radiol.12120485

Kirby M, Heydarian M, Wheatley A, McCormack DG, Parraga G (2012b) Evaluating bronchodilator effects in chronic obstructive pulmonary disease using diffusion-weighted hyperpolarized helium-3 magnetic resonance imaging. J Appl Physiol (1985) 112(4):651–657. doi:10.1152/japplphysiol.01295.2011

Kirby M, Svenningsen S, Kanhere N, Owrangi A, Wheatley A, Coxson HO et al (2013) Pulmonary ventilation visualized using hyperpolarized helium-3 and xenon-129 magnetic resonance imaging: differences in COPD and relationship to emphysema. J Appl Physiol (1985) 114(6):707–715. doi:10.1152/japplphysiol.01206.2012

Kohlmann P, Strehlow J, Jobst B, Krass S, Kuhnigk JM, Anjorin A et al (2015) Automatic lung segmentation method for MRI-based lung perfusion studies of patients with chronic obstructive pulmonary disease. Int J Comput Assist Radiol Surg 10(4):403–417. doi:10.1007/s11548-014-1090-0

Kruger SJ, Nagle SK, Couch MJ, Ohno Y, Albert M, Fain SB (2016) Functional imaging of the lungs with gas agents. J Magn Reson Imaging 43(2):295–315. doi:10.1002/jmri.25002

Lehmann F, Knitz F, Weiler N, Gast KK, Ley S, Schmiedeskamp J et al (2004) A software tool for analysis and quantification of regional pulmonary ventilation using dynamic hyperpolarised-(3)He-MRI. Fortschr Röntgenstr 176(10):1399–1408

Ley S, Zaporozhan J, Morbach A, Eberle B, Gast KK, Heussel CP et al (2004a) Functional evaluation of emphysema using diffusion-weighted 3Helium-

magnetic resonance imaging, high-resolution computed tomography, and lung function tests. Investig Radiol 39(7):427–434

Ley S, Fink C, Puderbach M, Plathow C, Risse F, Kreitner KF et al (2004b) Contrast-enhanced 3D MR perfusion of the lung: application of parallel imaging technique in healthy subjects. Fortschr Röntgenstr 176(3):330–334

Ley S, Puderbach M, Risse F, Ley-Zaporozhan J, Eichinger M, Takenaka D et al (2007) Impact of oxygen inhalation on the pulmonary circulation: assessment by magnetic resonance (MR)-perfusion and MR-flow measurements. Investig Radiol 42(5):283–290

Ley-Zaporozhan J, van Beek EJ (2010) Imaging phenotypes of chronic obstructive pulmonary disease. J Magn Reson Imaging 32(6):1340–1352. doi:10.1002/jmri.22376

Ley-Zaporozhan J, Ley S, Eberhardt R, Weinheimer O, Fink C, Puderbach M et al (2007) Assessment of the relationship between lung parenchymal destruction and impaired pulmonary perfusion on a lobar level in patients with emphysema. Eur J Radiol 63(1):76–83

Ley-Zaporozhan J, Puderbach M, Kauczor HU (2008) MR for the evaluation of obstructive pulmonary disease. Magn Reson Imaging Clin N Am 16(2):291–308

Ley-Zaporozhan J, Ley S, Eberhardt R, Kauczor HU, Heussel CP (2010) Visualization of morphological parenchymal changes in emphysema: comparison of different MRI sequences to 3D-HRCT. Eur J Radiol 73(1):43–49. doi:10.1016/j.Ejrad.2008.09.029

Ley-Zaporozhan J, Molinari F, Risse F, Puderbach M, Schenk JP, Kopp-Schneider A et al (2011) Repeatability and reproducibility of quantitative whole-lung perfusion magnetic resonance imaging. J Thorac Imaging 26(3):230–239. doi:10.1097/RTI.0b013e3181e48c36

Loffler R, Muller CJ, Peller M, Penzkofer H, Deimling M, Schwaiblmair M et al (2000) Optimization and evaluation of the signal intensity change in multisection oxygen-enhanced MR lung imaging. Magn Reson Med 43(6):860–866

Ma W, Sheikh K, Svenningsen S, Pike D, Guo F, Etemad-Rezai R et al (2015) Ultra-short echo-time pulmonary MRI: evaluation and reproducibility in COPD subjects with and without bronchiectasis. J Magn Reson Imaging 41(5):1465–1474. doi:10.1002/jmri.24680

Marshall H, Deppe MH, Parra-Robles J, Hillis S, Billings CG, Rajaram S et al (2012) Direct visualisation of collateral ventilation in COPD with hyperpolarised gas MRI. Thorax 67(7):613–617. doi:10.1136/thoraxjnl-2011-200864

Mathew L, Evans A, Ouriadov A, Etemad-Rezai R, Fogel R, Santyr G et al (2008) Hyperpolarized 3He magnetic resonance imaging of chronic obstructive pulmonary disease: reproducibility at 3.0 tesla. Acad Radiol 15(10):1298–1311. doi:10.1016/j.acra.2008.04.019

Mathew L, Kirby M, Etemad-Rezai R, Wheatley A, McCormack DG, Parraga G (2011) Hyperpolarized (3)He magnetic resonance imaging: preliminary evaluation of phenotyping potential in chronic obstructive pulmonary disease. Eur J Radiol 79(1):140–146. doi:10.1016/j.ejrad.2009.10.028

Molinari F, Fink C, Risse F, Tuengerthal S, Bonomo L, Kauczor HU (2006) Assessment of differential pulmonary blood flow using perfusion magnetic resonance imaging: comparison with radionuclide perfusion Scintigraphy. Investig Radiol 41(8):624–630

Moonen M, Xu J, Johansson A, Thylen A, Bake B (2005) Effects of lung volume reduction surgery on distribution of ventilation and perfusion. Clin Physiol Funct Imaging 25(3):152–157

Morbach AE, Gast KK, Schmiedeskamp J, Dahmen A, Herweling A, Heussel CP et al (2005) Diffusion-weighted MRI of the lung with hyperpolarized helium-3: a study of reproducibility. J Magn Reson Imaging 21(6):765–774

Morgan AR, Parker GJ, Roberts C, Buonaccorsi GA, Maguire NC, Hubbard Cristinacce PL et al (2014) Feasibility assessment of using oxygen-enhanced magnetic resonance imaging for evaluating the effect of pharmacological treatment in COPD. Eur J Radiol 83(11):2093–2101. doi:10.1016/j.Ejrad.2014.08.004

Morino S, Toba T, Araki M, Azuma T, Tsutsumi S, Tao H et al (2006) Noninvasive assessment of pulmonary emphysema using dynamic contrast-enhanced magnetic resonance imaging. Exp Lung Res 32(1–2):55–67

Muller CJ, Schwaiblmair M, Scheidler J, Deimling M, Weber J, Loffler RB et al (2002) Pulmonary diffusing capacity: assessment with oxygen-enhanced lung MR imaging preliminary findings. Radiology 222(2):499–506

Ohno Y, Chen Q, Hatabu H (2001) Oxygen-enhanced magnetic resonance ventilation imaging of lung. Eur J Radiol 37(3):164–171

Ohno Y, Sugimura K, Hatabu H (2003) Clinical oxygen-enhanced magnetic resonance imaging of the lung. Top Magn Reson Imaging 14(3):237–243

Ohno Y, Hatabu H, Higashino T, Takenaka D, Watanabe H, Nishimura Y et al (2004a) Dynamic perfusion MRI versus perfusion scintigraphy: prediction of postoperative lung function in patients with lung cancer. AJR Am J Roentgenol 182(1):73–78

Ohno Y, Hatabu H, Murase K, Higashino T, Kawamitsu H, Watanabe H et al (2004b) Quantitative assessment of regional pulmonary perfusion in the entire lung using three-dimensional ultrafast dynamic contrast-enhanced magnetic resonance imaging: preliminary

experience in 40 subjects. J Magn Reson Imaging 20(3):353–365

Ohno Y, Koyama H, Nogami M, Takenaka D, Matsumoto S, Obara M et al (2008a) Dynamic oxygen-enhanced MRI versus quantitative CT: pulmonary functional loss assessment and clinical stage classification of smoking-related COPD. AJR Am J Roentgenol 190(2):W93–W99. doi:10.2214/AJR.07.2511

Ohno Y, Iwasawa T, Seo JB, Koyama H, Takahashi H, Oh YM et al (2008b) Oxygen-enhanced magnetic resonance imaging versus computed tomography: multicenter study for clinical stage classification of smoking-related chronic obstructive pulmonary disease. Am J Respir Crit Care Med 177(10):1095–1102. doi:10.1164/rccm.200709-1322OC

Ohno Y, Koyama H, Yoshikawa T, Matsumoto K, Takahashi M, Van Cauteren M et al (2011) T2* measurements of 3-T MRI with ultrashort TEs: capabilities of pulmonary function assessment and clinical stage classification in smokers. AJR Am J Roentgenol 197(2):W279–W285. doi:10.2214/AJR.10.5350

Ohno Y, Koyama H, Yoshikawa T, Matsumoto K, Aoyama N, Onishi Y et al (2012) Comparison of capability of dynamic O(2)-enhanced MRI and quantitative thin-section MDCT to assess COPD in smokers. Eur J Radiol 81(5):1068–1075. doi:10.1016/j.ejrad.2011.02.004

Ohno Y, Nishio M, Koyama H, Yoshikawa T, Matsumoto S, Seki S et al (2014) Pulmonary 3 T MRI with ultrashort TEs: influence of ultrashort echo time interval on pulmonary functional and clinical stage assessments of smokers. J Magn Reson Imaging 39(4):988–997. doi:10.1002/jmri.24232

Pennati F, Quirk JD, Yablonskiy DA, Castro M, Aliverti A, Woods JC (2014) Assessment of regional lung function with multivolume (1)H MR imaging in health and obstructive lung disease: comparison with (3)He MR imaging. Radiology 273(2):580–590. doi:10.1148/radiol.14132470

Plathow C, Fink C, Ley S, Puderbach M, Eichinger M, Schmahl A et al (2004) Measurement of diaphragmatic length during the breathing cycle by dynamic MRI: comparison between healthy adults and patients with an intrathoracic tumor. Eur Radiol 14(8):1392–1399

Plathow C, Schoebinger M, Fink C, Ley S, Puderbach M, Eichinger M et al (2005) Evaluation of lung volumetry using dynamic three-dimensional magnetic resonance imaging. Invest Radiol 40(3):173–179

Rabe KF, Hurd S, Anzueto A, Barnes PJ, Buist SA, Calverley P et al (2007) Global strategy for the diagnosis, management, and prevention of chronic obstructive pulmonary disease: GOLD executive summary. Am J Respir Crit Care Med 176(6):532–555

Roach DJ, Cremillieux Y, Serai SD, Thomen RP, Wang H, Zou Y et al (2016) Morphological and quantitative evaluation of emphysema in chronic obstructive pulmonary disease patients: a comparative study of MRI with CT. J Magn Reson Imaging 44(6):1656–1663. doi:10.1002/jmri.25309

Rosenkranz S (2007) Pulmonary hypertension: current diagnosis and treatment. Clin Res Cardiol 96:527–541

Salerno M, Altes TA, Brookeman JR, de Lange EE, Mugler JP III (2001) Dynamic spiral MRI of pulmonary gas flow using hyperpolarized (3)He: preliminary studies in healthy and diseased lungs. Magn Reson Med 46(4):667–677

Salerno M, de Lange EE, Altes TA, Truwit JD, Brookeman JR, Mugler JP III (2002) Emphysema: hyperpolarized helium 3 diffusion MR imaging of the lungs compared with spirometric indexes – initial experience. Radiology 222(1):252–260

Sandek K, Bratel T, Lagerstrand L, Rosell H (2002) Relationship between lung function, ventilation-perfusion inequality and extent of emphysema as assessed by high-resolution computed tomography. Respir Med 96(11):934–943

Schuster DP, Marklin GF (1986) Effect of changes in inflation and blood volume on regional lung density – a PET study: 2. J Comput Assist Tomogr 10(5):730–735

Sergiacomi G, Sodani G, Fabiano S, Manenti G, Spinelli A, Konda D et al (2003) MRI lung perfusion 2D dynamic breath-hold technique in patients with severe emphysema. In vivo 17(4):319–324

Sergiacomi G, Taglieri A, Chiaravalloti A, Calabria E, Arduini S, Tosti D et al (2014) Acute COPD exacerbation: 3 T MRI evaluation of pulmonary regional perfusion – preliminary experience. Respir Med 108(6):875–882. doi:10.1016/j.rmed.2014.04.002

Stadler A, Jakob PM, Griswold M, Stiebellehner L, Barth M, Bankier AA (2008) T(1) mapping of the entire lung parenchyma: influence of respiratory phase and correlation to lung function test results in patients with diffuse lung disease. Magn Reson med 59(1):96–101

Suga K, Tsukuda T, Awaya H, Takano K, Koike S, Matsunaga N et al (1999) Impaired respiratory mechanics in pulmonary emphysema: evaluation with dynamic breathing MRI. J Magn Reson Imaging 10(4):510–520

Swift AJ, Wild JM, Fichele S, Woodhouse N, Fleming S, Waterhouse J et al (2005) Emphysematous changes and normal variation in smokers and COPD patients using diffusion 3He MRI. Eur J Radiol 54(3):352–358

Swift AJ, Woodhouse N, Fichele S, Siedel J, Mills GH, van Beek EJ et al (2007) Rapid lung volumetry using ultrafast dynamic magnetic resonance imaging during forced vital capacity maneuver: correlation with spirometry. Invest Radiol 42(1):37–41

Szilasi M, Dolinay T, Nemes Z, Strausz J (2006) Pathology of chronic obstructive pulmonary disease. Pathol Oncol Res 12(1):52–60

Thabut G, Dauriat G, Stern JB, Logeart D, Levy A, Marrash-Chahla R et al (2005) Pulmonary hemody-

namics in advanced COPD candidates for lung vol-
ume reduction surgery or lung transplantation. Chest
127(5):1531–1536

Virgincar RS, Cleveland ZI, Kaushik SS, Freeman MS,
Nouls J, Cofer GP et al (2013) Quantitative analysis of
hyperpolarized 129Xe ventilation imaging in healthy
volunteers and subjects with chronic obstructive
pulmonary disease. NMR Biomed 26(4):424–435.
doi:10.1002/nbm.2880

Vonk Noordegraaf A, Marcus JT, Roseboom B, Postmus
PE, Faes TJ, de Vries PM (1997) The effect of right
ventricular hypertrophy on left ventricular ejection frac-
tion in pulmonary emphysema. Chest 112(3):640–645

Vonk-Noordegraaf A, Marcus JT, Holverda S, Roseboom
B, Postmus PE (2005) Early changes of cardiac struc-
ture and function in COPD patients with mild hypox-
emia. Chest 127(6):1898–1903

Weitzenblum E, Chaouat A (2005) Severe pulmonary
hypertension in COPD: is it a distinct disease? Chest
127(5):1480–1482

Wild JM, Paley MN, Kasuboski L, Swift A, Fichele S,
Woodhouse N et al (2003) Dynamic radial projection
MRI of inhaled hyperpolarized 3He gas. Magn Reson
Med 49(6):991–997

Zaporozhan J, Ley S, Gast KK, Schmiedeskamp J,
Biedermann A, Eberle B et al (2004) Functional anal-
ysis in single-lung transplant recipients: a comparative
study of high-resolution CT, (3)He-MRI, and pulmo-
nary function tests. Chest 125(1):173–181